Rajapakse Chamith (Orcid ID: 0000-0002-9247-833X)

Effect of Low Intensity Vibration on Bone Strength, Microstructure, and Adiposity in Pre-Osteoporotic Postmenopausal Women: A Randomized Placebo-Controlled Trial

Chamith S. Rajapakse[1, 2], Alyssa J. Johncola[1], Alexandra S. Batzdorf[1], Brandon C. Jones[1], Mona Al Mukaddam[2, 3], Kelly Sexton[1], Justine Shults[4], Mary B. Leonard[5, 6], Peter J. Snyder[3], and Felix W. Wehrli[1]

[1] Department of Radiology, University of Pennsylvania, Philadelphia, PA

[2] Department of Orthopaedic Surgery, University of Pennsylvania, Philadelphia, PA

[3] Department of Medicine, University of Pennsylvania, Philadelphia, PA

[4] Department of Biostatistics, Epidemiology and Informatics, University of Pennsylvania, Philadelphia, PA

[5] Department of Pediatrics, Children's Hospital of Philadelphia, University of Pennsylvania, Philadelphia, PA

[6] Current Affiliation: Department of Pediatrics, Stanford University School of Medicine, Stanford, CA

Corresponding Author:

Chamith S. Rajapakse, Ph.D.

Department of Radiology

University of Pennsylvania School of Medicine

3400 Spruce Street, 1 Founders Building

Philadelphia, PA 19104

Telephone: 215-349-8519

Email: chamith@pennmedicine.upenn.edu

This article has been accepted for publication and undergone full peer review but has not been through the copyediting, typesetting, pagination and proofreading process which may lead to differences between this version and the Version of Record. Please cite this article as doi: 10.1002/jbmr.4229

Acknowledgements: This work was supported by grants from the National Institutes of Health: R01 AR055647, R01 AR068382, and R01 AR076392.

Abstract

There has been evidence that cyclical mechanical stimulation may be osteogenic, thus providing opportunities for non-pharmacological treatment of degenerative bone disease. Here, we applied this technology to a cohort of postmenopausal women with varying bone mineral density (BMD) T-scores at the total hip (-0.524±0.843) and spine (-0.795±1.03) to examine the response to intervention after one year of daily treatment with ten minutes of vibration therapy in a randomized double-blinded trial. The device operates either in an active mode (30 Hz and 0.3 g) or placebo. Primary endpoints were changes in bone stiffness at the distal tibia and marrow adiposity of the vertebrae, based on 3 Tesla high-resolution MRI and spectroscopic imaging, respectively. Secondary outcome variables included distal tibial trabecular microstructural parameters and vertebral deformity determined by MRI, volumetric and areal bone densities derived using peripheral quantitative computed tomography (pQCT) of the tibia, and dual-energy X-ray absorptiometry (DXA)-based BMD of the hip and spine. Device adherence was 83% in the active group (n=42) and 86% in the placebo group (n=38), and did not differ between groups (p=0.7). The mean 12-month changes in tibial stiffness in the treatment group and placebo group were +1.31 ± 6.05 and -2.55 ± 3.90 %, respectively (group difference 3.86%, p=0.0096). In the active group, marrow fat fraction significantly decreased after 12 months of intervention (p=0.0003), while no significant change was observed in the placebo group (p=0.7; group difference -1.59 %, p=0.029). Mean differences of the changes in trabecular bone volume fraction (p=0.048) and erosion index (p=0.044) were also significant, as was pQCT-derived trabecular volumetric BMD (vBMD; p=0.016) at the tibia. The data are commensurate with the hypothesis that vibration therapy is protective against loss in mechanical strength, and further,

that the intervention minimizes the shift from the osteoblastic to the adipocytic lineage of mesenchymal stem cells.

Keywords: Vibration Therapy, Bone, Osteoporosis, MRI

Introduction

Osteoporosis and osteopenia (precursor of osteoporosis, represented by low bone mass) are major public health threats for 44 million people in the U.S. aged 50 and older. Fortunately, effective treatment has been available for two decades in the form of a spectrum of antiresorptive and anabolic drugs [1]. However, pharmacological intervention can be associated with side effects, decreasing adherence and increasing the desire for non-pharmacological interventions. For example, oral bisphosphonates are not well tolerated by patients with gastric reflux problems [2]. Further, the risk of osteonecrosis of the jaw and atypical femur fracture resulting from bisphosphonate treatment, while comparatively rare, remains a concern for patients undergoing long-term treatment [3]. Newer, more powerful treatments, such as zoledronic acid, an intravenous bisphosphonate administered once a year, have significant side effects, including fever with flu-like symptoms lasting several days upon injection, are not uncommon. Additional risks, while rare, include atrial fibrillation [4]. New osteoanabolic agents such as Abaloparatide or Romosozumab are approved for use for only 24 months and 12 months, respectively, highlighting the need for safe and effective agents that could be used long-term [5].

It is well known that a sedentary life style predisposes people to bone loss and, conversely, that weight-bearing exercise has an osteogenic effect by reducing bone resorption and enhancing bone formation [6, 7]. Specifically, it has been shown that mechanical loading down-regulates the nuclear hormone receptor, peroxisome proliferator-activated receptor gamma (PPARγ), in bone marrow stromal cells, thereby committing their differentiation toward

osteoblasts instead of adipocytes [8]. PPARγ is well known to play a key role in adipocyte-specific gene expression. It is therefore plausible that decreased adipogenesis is the cause underlying osteogenesis induced by mechanical stimulation.

Paralleling the results of work on cells, Rubin et al. showed in mice that cyclical mechanical stimulation reduced commitment of mesenchymal stem cells toward adipocytes by inhibiting adipogenesis by 27% [9]. The observation of an inverse relationship between bone marrow fat content and bone density, including in early work by some of the present authors, is thus not surprising[10-12]. It has been known for almost two decades that low-frequency, low-amplitude mechanical stimulation is osteogenic in animals [13-15]. While most animal studies showing an effect used young females, it is possible that growing bone behaves differently from mature bone. Subsequently, there has been evidence that this may be the case in humans, as well [16]. The mechanobiology underlying these phenomena is beginning to emerge in terms of expression of genes stimulated by the action of the vibration as shown in osteocyte cell cultures [17]. Arnsdorf et al. demonstrated that mechanical stimulation alters the epigenetic state of promoter regions of three osteogenic genes from marrow-derived mesenchymal stem cells by reducing DNA methylation, thereby causing an associated increase in their expression [18]. Further, it is known that sclerostin, a protein secreted by osteocytes, is a potent inhibitor of bone formation. Robling et al. showed that mechanical loading *in vivo* downregulates sclerostin expression with concomitant enhanced bone formation [19].

Rubin et al found very small forces—corresponding to 0.3g (1g=9.81 m/s^2)—resulting in very small strain levels on the order of 5-10 microstrains to be osteogenic [20]. Subsequent work by Judex et al. indicated that high-resolution imaging-based finite-element analysis of trabecular bone samples can detect adaptation of the trabecular bone network in sheep treated with low-

intensity vibration, but not in controls [21]. Even though initial trials in humans treated by what has subsequently been referred to as low-magnitude mechanical stimulation showed an anabolic response [22-27], it was far less than that previously reported in sheep [28], and in fact, in some trials, no effect was found [29] (see also [30] for a recent meta-analysis examining the effectiveness of vibration treatment). More recent data [31], including a pilot study conducted in the authors' laboratory [32], clearly showed significant, albeit small, effects detectable by some, but not all, diagnostic imaging modalities. Both these studies further highlight the importance of using diagnostic techniques sensitive to subtle changes in bone microstructure, as well as the critical role of patient adherence.

Here, we report the results of a double-blind, prospective trial in postmenopausal women with low bone density to address the hypothesis that bone quality measured in terms of MRI-derived strength, microstructure, and adiposity is improved by daily application of low-intensity vibration, relative to placebo.

Methods

Study Participants

This prospective, randomized, double-blinded, 12-month study (ClinicalTrials.gov identifier: NCT01921517) was approved by the authors' institutional review board (IRB) and complied with Health Insurance Portability and Accountability Act (HIPAA) guidelines. All study participants provided written informed consent. Recruitment strategies included mass mailings, study flyers, study brochures, and Penn Media services, including Express Weekly, a blast email system. The Penn Data Store was utilized for the mass mailings to target potential subjects within a 30-mile radius of the University of Pennsylvania. Our first and last randomized participants were enrolled in April 2014 and October 2017, respectively. Follow-up study visits

continued into 2018. Postmenopausal females aged 45 – 65 years were eligible for the study. Postmenopausal status was defined by a history of amenorrhea for a minimum of 24 months, a serum follicle-stimulating hormone (FSH) concentration of at least 25 mIU/mL (milli-International unit per milliliter), and a negative pregnancy test. Exclusion criteria were current or prior use of medications known to affect bone (e.g., bisphosphonates, calcitonin, selective estrogen receptor modulators, denosumab, diphenylhydantoin, recent systemic glucocorticoids), dual-energy X-ray absorptiometry (DXA) bone mineral density (BMD) T-score of less than -2.5 or greater than +2.0, vitamin D level less than 12 ng/mL, body mass index (BMI) of greater than 32, current alcohol or drug abuse (more than three alcoholic beverages per day or current abuse of illicit drugs or prescription medication), uncontrolled or untreated cardiac or pulmonary disease, liver disease (history of hepatitis or alanine aminotransferase or aspartate aminotransferase greater than twice the upper limit of normal), renal disease (history of renal disease or serum creatinine greater than twice the upper limit of normal), diabetes, and contraindication to magnetic resonance imaging (MRI; e.g., pacemaker, metallic implants, claustrophobia).

Randomization

Subjects meeting the entry criteria at the screening visit were randomly allocated 1:1 to either an active low-intensity vibration or placebo device designed for home use. Random numbers were generated using a random number generator by the statistician, who maintained a database with even numbers being assigned to treatment and odd numbers to placebo. Each subject was assigned a study number. Subjects' names and study numbers were kept by the statistician in a password-protected database separate from other study records and were not shared with the P.I. or other members of the study team. The research coordinator who instructed the participants on

how use the device was not involved in the assessment of study outcomes. All other investigators and participants were blinded to device assignment.

Intervention

The vibration device used is essentially identical to that described in prior studies [31]. Briefly, the device, which resembles a large bathroom scale, oscillates in the vertical direction at a frequency of 30 Hz with 0.3g acceleration, requiring a displacement of approximately 90 μm. Similar device parameters have been shown previously to induce anabolic bone microstructural changes in large animal experiments [14] and, most recently, in a randomized placebo control study of children with Crohn's disease [31] and a pilot human study by some of the present investigators [33]. An accelerometer fixed to the top plate provides a closed-loop feedback signal to maintain the vibration intensity at a constant value throughout the intervention period. The actuator of the placebo device is inactive, but is indistinguishable from the active device in appearance and operation. A small speaker connected to all devices emits a 500 Hz audible tone to mask the active/placebo status. Participants were instructed to stand on the platform in a relaxed stance, with knees neither locked nor bent, either barefoot or wearing stockings for ten minutes daily over a 12-month period. The device is designed to induce the maximum possible amplitude of stimulation all the way up to the spine with a given vibrational load at the feet [34].

Adherence Monitoring

An onboard electronic adherence monitoring system recorded the date, time, and duration of device use as well as subjects' weight. Participants were also asked to maintain a log book to record daily device use times. Adherence feedback was provided to study participants in bi-weekly intervals by the study coordinators through phone calls. Subjects were also monitored in person at three- and six-month visits to review adherence and to record adverse events. At the

end of the trial, the devices were returned to the study coordinator and the adherence data were extracted. Adherence was assumed to be 100% if the total number of minutes using the device during the 1-year period was 365 x 10 mins, paralleling the report by Gilsanz et al [23].

Outcome Measures

The distal tibia (3% up the tibia) was chosen as the primary site for bone microstructure and stiffness measurements because of the proximity to the external mechanical stimulus applied to the feet and because it is a site rich in trabecular bone. Cortical bone measurements were performed at the mid tibia, 38% up the tibia, as this is the thickest part of a load-bearing bone on the direct transmission path of the vibration signals. Standard-of-care BMD tests were conducted for the total hip and lumbar spine, as is routinely performed clinically. Bone marrow composition was assessed at the lumbar spine, a site known for age-related changes in fat fraction [35]. Vertebral deformities were assessed in the total spine, as age-related deformity fractures could occur any part of the spine.

Imaging Procedures

All subjects underwent a series of imaging procedures involving MRI at the tibia and spine, DXA of the hip and spine, and peripheral quantitative computed tomography (pQCT) at the tibia, as described below. Details of the procedures are illustrated in **Figure 1**.

Magnetic Resonance Imaging

Participants were imaged on a 3 Tesla whole-body MRI scanner (Siemens TIM Trio, Erlangen, Germany) in feet-first, supine position. Left distal tibia metaphysis (3% site) bone microstructure was imaged using a four-channel, receive-only, phased-array radio-frequency coil (Insight MRI, Worcester, MA), paralleling the setup described by Wald et al. [36]. Prospective registration was used to prescribe matching imaging volumes between baseline and follow-up scan sessions [37].

The scan protocol consisted of the fast large-angle spin echo (FLASE) pulse sequence [38], field of view 70x63x13 mm^3 (third dimension being inferosuperior), flip angle of 140°, repetition time/echo time 60/11 ms, 137x137x410 μm^3 voxel size, and acquisition time 6 min 15 s.

Vertebral bone marrow scanning was performed with the system's standard spine array using a chemical shift imaging sequence [39]. The sequence included a 90°-180° radio frequency pulse pair, followed by 16 equal-polarity gradient echoes, the first coinciding with the spin echo. The sequence was played out as six interleaved gradient-echo trains, offset in time by 0.6 ms, corresponding to a spectral bandwidth of 1.67 kHz. Three saturation bands were placed anteriorly to the imaging volume to minimize abdominal motion artifacts. Sequence parameters used were repetition time 1,000 ms, spin echo time 8 ms, echo spacing 6 ms, field of view 30 cm x 60 cm, matrix size 60 x 120, slice thickness 10 mm, and acquisition time 12.8 mins.

Vertebral deformity imaging was performed with the aforementioned spine array using a fast spin echo sequence with repetition time/echo time 1500/70 ms, three excitations, field of view 40×30 cm, pixel size 0.78 mm x 1.0 mm, and eight 5-mm sagittal slices.

MRI Distal Tibia Analysis

Retrospective image registration was performed between baseline and follow-up images to select closely matching 8-mm trans-axial bone segments for analysis [37]. Whole-bone and trabecular compartments were extracted for analysis by delineating the periosteal and endosteal boundaries [40]. Whole cross-section stiffness was computed using finite-element analysis by simulating loading in the inferosuperior direction [32, 40, 41]. At each voxel, tissue modulus was assumed to be (bone-volume fraction) x 15 GPa and Poisson's ratio was set to 0.3. Axial displacements corresponding to 1% strain was applied and the stiffness was calculated as the ratio of reaction force and displacement. Stiffness is a measure of bone strength, which is a function of

microstructure and other bone quality parameters. Bone stiffness decreases with aging after menopause, predisposing these subjects to increased fracture risk. Bone volume fraction (BV/TV) in the trabecular bone compartment was calculated as the average of the voxel BV/TV. Bone microstructure was assessed using digital topological analysis through surface-to-curve ratio, a measure of plate-likeness versus rod-likeness of trabecular bone network, and erosion index, a marker of osteoclastic resorption of trabeculae [42].

MRI Vertebral Fat Analysis

Complex imaging data were ordered in time, resulting in 96 data points for each pixel, followed by zero filling to 256 points, apodization filtering, and one-dimensional Fourier transform along the time axis to obtain absorption-mode spectra at each pixel. Relative fat (F) and water (W) content were calculated by integrating the spectra from 0–3 ppm and from 3.5–6 ppm, respectively. Fat fraction maps were created by assigning the corresponding F/(F +W) value at each pixel. The bone marrow region was manually selected to calculate the average fat fraction at each vertebral level. Lumbar marrow fat fraction was calculated by averaging the fat fraction across L1-L5 vertebrae.

MRI Vertebral Deformity Quantification

A stack of sagittal fast spin-echo MR images guided the vertebral deformity analysis [43]. The image transecting each vertebra in the midline was located and the spatial coordinates of the anterior, middle, and posterior points of the inferior and superior edges of the vertebra were manually marked, avoiding errors from osteophytes and depressions caused by endplate herniations (Schmorl's nodes). Anterior (H_a), middle (H_m), and posterior (H_p) heights of each vertebra were calculated by taking the Euclidian distance between landmark points. Three types of vertebral deformities were calculated as wedge ([Hp/Ha − 1] × 100%]), biconcavity ([Hp/Hm

− 1] × 100%]), and crush ([average neighboring vertebral heights] / [average current vertebral heights] – 1] × 100%) deformities. The total thoracolumbar deformity was defined as the average of all three types of deformity from T1 to L5 vertebrae.

pQCT

Left tibia BMD was obtained by pQCT (Stratec XCT 2000 12-detector unit, Orthometrix, Inc.) at a voxel size of 0.4 mm, slice thickness of 2.3 mm, and scan speed of 25 mm/s and processed using Stratec software version 6.00 [44]. Volumetric trabecular and cortical densities were derived from the 3% metaphyseal and 38% diaphyseal sites, respectively. A hydroxyapatite phantom was scanned daily to provide quality control. The *in vivo* coefficient of variation ranged from 0.5-1.6% for pQCT measures [45].

DXA

Left total-hip and posteroanterior lumbar spine (L1-L4) areal BMD (aBMD) were measured using DXA (Delphi/Discovery Densitometer, Hologic, Inc., Marlborough, MA) in the array mode using standard positioning techniques. This instrument was calibrated using a hydroxyapatite spine phantom daily and whole-body phantom three times per week. The coefficient of variation for both *in-vitro* phantom scans and *in vivo* spine scans is < 1% [46].

Statistical Analysis

Group differences in temporal change in variables between active and placebo arms were evaluated via unpaired two-sided t-tests or nonparametric Wilcoxon signed-rank tests for normally and not normally distributed data, respectively. Within-group temporal changes in parameters were assessed using paired two-sided t-tests when data were normally distributed or nonparametric Wilcoxon signed-rank tests otherwise. Inter-parameter correlations were evaluated using Pearson correlation when data were normally distributed and Spearman

correlation when data were not normally distributed. A full intention-to-treat analysis can only be performed where complete outcome data are available for all randomized subjects. However, due to dropouts some randomized subjects did not return for the 12-month follow-up visit. Therefore, per-protocol analysis was performed for all subjects that had both baseline and follow-up data. All analyses were performed using JMP Statistical Discovery Software, Version 15.0.0 (SAS Institute, Inc., Cary, NC), with $p<0.05$ indicating statistical significance.

The coefficient of variation for MRI measured stiffness (primary outcome variable) and bone marrow fat fraction (secondary outcome variable) is 4% [36, 47] and 2%, respectively. Gilsanz et al. found a group difference between treatment and placebo subjects of 3.9% for vertebral trabecular BMD for those using a vibration device for at least two minutes per day [23]. Furthermore, longitudinal change in stiffness is always greater than a commensurate change in bone volume fraction (or BMD). We conservatively estimated that an effect on the order of 3%, corresponding to a standardized effect size of 0.77, would require 37 subjects per group for a two-sided unpaired t-test for a type-one error rate of 5% and 90% power. Enrolment was discontinued after 80 subjects were randomized between the two groups in agreement with the funding timeline.

Results

Participant Characteristics

For this randomized trial, a total of 415 women were telephone screened, of which 182 (44%) were eligible for a screening visit (**Fig. 2**). Of these, 117 (64%) women completed the screening visit and 87 (74%) were eligible based on DXA, BMI, and lab criteria. Eighty (92%) were randomized, with 42 (52%) being given active devices and 38 (48%) being given placebo devices. The enrollment data of this double-blinded intervention trial show that the subjects were

well matched between groups. Baseline demographics, bone and body composition measurements, and device adherence did not significantly differ between treatment arms (**Table 1**). There was no evidence that the participants could correctly guess their treatment assignment and no adverse events related to the device use were reported.

A total of 25 (60%) and 29 (76%) participants respectively from the active and placebo arms completed the 12-month visit (68% total retention). The 12-month median (interquartile range) adherence to device use was 83.0 (62.3 – 91.1) and 86.1 (63.1 – 93.2) percent in the active and placebo arms, respectively, and did not differ between the two groups (p=0.72). The majority of the participants logged 10 mins of device usage each day according to the data captured by the onboard monitoring system. Only two subjects showed overall adherence < 20%, corresponding to 2m/d. If 0% adherence was assumed to participants whose data were not available due to dropout, an intention-to-treat analysis (not possible since there is no data available) mean (median) adherence would be 56% (78%) and 65% (75%) in the active and placebo arms, respectively. Of particular importance, such a high adherence makes the results particularly meaningful. None of the baseline demographics, imaging, or other parameters were significantly different ($p>0.05$) between dropouts in the two treatment arms and the subjects having undergone the complete protocol, reassuring that no selection bias was introduced due to subjects lost.

Primary and Secondary Outcomes

The two primary outcome variables examined were computationally quantified stiffness of the distal tibia bone obtained from MRI-derived bone structure, and independently, a measure of marrow metabolism, the vertebral bone marrow's adiposity. Additional secondary variables included DXA bone densities of the spine and hip, as well as pQCT measures at the distal tibia,

and vertebral deformity. Co-registered baseline and follow-up image pairs allowed the assessment of closely matched anatomical regions (**Fig. 3**). **Table 2** lists the changes of the outcome variables based on per-protocol analysis in placebo and treatment group after the 12-month intervention period involving ten minutes of daily exposure to vibration therapy. The difference of the mean change in stiffness between groups was significant ($p<0.01$), as was the mean change in vertebral marrow adiposity ($p<0.05$), with the signs of both differential changes supporting the hypothesis. Mean changes in several secondary variables were significant, as well. These include structural parameters evaluated by high-resolution MRI such as BV/TV and erosion index (a topological quantity of the trabecular network), and trabecular vBMD obtained by pQCT (all $p<0.05$). Interestingly, DXA aBMD at the total hip and lumbar spine did not demonstrate any treatment effect, nor was there any difference in vertebral deformity.

Within-Group Changes

Table 3 reports baseline and 12-month follow-up data for each group. While stiffness declined in the placebo group ($p=0.004$), there was no detectable change in the treatment group. Structural parameters (surface-to-curve ratio and erosion index), which are measures of the integrity of the trabecular network, seemed to improve in the treatment group, but only the erosion index declined significantly ($p=0.004$), with no detectable changes in the placebo group. The data further indicate a reduction in vertebral marrow adiposity in the active group ($p=0.0003$), but not the placebo group ($p=0.71$). The only densitometric parameter that demonstrated a longitudinal effect was total hip DXA aBMD, which declined in the placebo group ($p=0.02$). The bar graph in **Figure 4** summarizes the results in terms of changes in parameters during the 12-month treatment period. It is worth noting the generally opposite trends in outcome variables between placebo and active groups.

Effect of Baseline Bone Health on Treatment Effect

Change in the primary outcome variable (i.e., tibia stiffness) was associated with a number of baseline bone measures. In the active arm, participants with poor baseline bone stiffness, BV/TV, surface-to-curve ratio, erosion index, fat fraction, and aBMD showed a greater response to the intervention than those who started off with good bone health (**Table 4**, **Fig. 5**). In the placebo arm, no such associations were observed except for the baseline spine aBMD, which indicates that having weak bone density is a risk factor for accelerated loss of stiffness if untreated. Baseline bone stiffness, lumbar fat fraction, and lumbar aBMD had significantly different associations with change in bone stiffness between the two treatment arms. Overall, these observations imply that subjects with the greatest deficits in mechanical or structural parameters elicited the largest treatment response.

Discussion

This prospective, randomized, double-blinded, 12-month trial of ten minutes of daily low-intensity vibration in pre-osteoporotic, postmenopausal women demonstrated beneficial effects on MRI-derived distal tibia stiffness, trabecular microstructure, and lumbar vertebral adiposity. Some treatment response was also observed in the pQCT-derived trabecular vBMD at the distal tibia. Interestingly, however, standard-of-care osteoporosis assessment by DXA did not show any significant improvement in aBMD at the lumbar spine, while total hip aBMD was unchanged in the treatment group and decreased in the placebo arm.

Post-hoc analysis revealed an inverse correlation between baseline bone quality metrics and treatment-induced changes. Specifically, participants who had low bone quality indices at

the initiation of the intervention showed the greatest response to treatment compared to those with better bone health, suggesting a possible ceiling effect. On the other hand, baseline bone measures were not significantly associated with the changes in outcome parameters in the placebo arm. It should be noted that most previous studies that reported beneficial effects of low-intensity vibration intervention involved cohorts with severely compromised bone quality at baseline. For example, vibration interventions have been found to be beneficial in patients with renal osteodystrophy [33], disabling conditions [25], idiopathic scoliosis [26], cerebral palsy [27], Crohn's disease [31], Rett syndrome [48], child cancer survivors [49], and young women (15 – 20 years) with low BMD and a history of bone fracture [23]. These studies, taken together with the results of the present work, suggest that low-intensity vibration may be best suited for individuals with compromised bone quality lacking regular stimulatory cues. Vibration therapy may thus serve as a potential surrogate for exercise. Previous studies that failed to demonstrate osteogenic effects of low-intensity vibration in healthy adults did so perhaps because the adults were already experiencing the stimulatory mechanical signals during normal ambulation or daily physical activity. Data from our study suggest that exogenous stimulation in the form of low-amplitude cyclical loading could be beneficial by slowing down postmenopausal bone loss in otherwise healthy women, especially those who might face barriers to regular exercise.

In a one-year , prospective, randomized, double-blind, and placebo- controlled trial , Rubin et al. reported that low-intensity vibration inhibited deterioration of bone in the spine and femur, even in healthy postmenopausal women, as long as device adherence was at least 80% [16]. Our data in non-osteoporotic postmenopausal women showed that this form of mechanical stimulation could not only inhibit bone loss, but improve measures of bone quality, the most relevant being mechanical competence assessed using computational biomechanics. Importantly,

our work did not require adjustments for adherence as a covariate, since overall adherence was high, with a median [IQR] of 83% [62% – 91%]. In contrast, Slatkovska et al. reported no significant effect of low-intensity vibration on bone density or structure measured by high-resolution pQCT (HR-pQCT) in postmenopausal women enrolled in a one-year, randomized, controlled trial, either at the distal tibia or radius [50]. The adherence in that study was bimodal, with most participants close to either 100% or 0% adherence [41% – 91% IQR]. Similarly, a study in men and women (ages 65 – 102 years) using the same vibration device did not show any benefit of ten minutes of daily exposure after 24 months in terms of QCT-derived volumetric vBMD at the hip and spine [29]. The adherence in that study was 68%. On the other hand, recent studies have highlighted the benefit of this form of intervention, with efficacy increasing with greater adherence [23, 31, 33, 48, 49]. More reliable adherence monitoring was possible in our study due to the recording electronics inside the vibrating platforms, rather than using self-reported device usage data. Further, routine communication between the participants and research coordinators might have positively affected adherence achieved in our study.

MRI has not been used previously to evaluate the effectiveness of vibration therapy on bone, except in a small pilot study in patients on dialysis conducted in the authors' laboratory [33]. MRI-based assessment of bone microstructure and strength has proven potential to detect subtle, short-term changes in response to intervention or disease progression or regression [37, 47, 51, 52]. Other benefits include superior soft-tissue contrast, absence of ionizing radiation, high repeat reproducibility, and wide availability.

The distal tibia has a spatially non-uniform trabecular microenvironment in all three spatial directions. Thus, small positional or rotational shifts in the choice of the imaging region between baseline and follow-up scans could introduce substantial errors masking true effects.

Here, we utilized prospective registration that ensures acquisition of matching imaging volumes for longitudinal bone micro-imaging studies with six degrees of adjustment (three positional and three rotational), even when the subject's leg was not positioned exactly the same for baseline and follow-up scans [37]. Such an approach further avoids interpolation-induced errors that could result from retrospectively registering the baseline and follow-up images.

In contrast to other low-intensity vibration studies that relied mainly on bone density as the primary endpoint, we used finite-element-derived whole-tibia stiffness as the primary outcome variable, a parameter that showed the most significant treatment effect compared to conventional measures of bone. Previous studies have also demonstrated that MRI-based finite-element analysis is sensitive to changes and differences in bone not captured by more traditional parameters focusing on bone volume and architecture [53, 54].

Importantly, our data provide compelling new evidence supporting the hypothesis that the intervention reduces lumbar bone marrow adiposity quantified by spectroscopic imaging, [55] indicating enhanced commitment of mesenchymal stem cells toward the osteoblastic lineage via downregulation of the nuclear hormone receptor, PPARγ, and thus suggesting a reduction in the rate of marrow adipogenesis to some degree, thereby retaining or enhancing the capacity for osteoblastogenesis. Inhibition of adipogenesis by mechanical stimulation has previously been demonstrated in stromal cells and rats *in vivo*, where animals running on a treadmill were compared to their stationary counterparts, showing both downregulation in PPARγ and reduction in marrow adipocyte volume in the exercise group [8]. A subsequent study in mice found that 15 weeks of 15 minutes of daily exposure to cyclical loading at 90 Hz via a vibrating platform similar to the one used in the present study inhibited adipogenesis by 27% [9]. While the effect in our work, which is the first to be detected in humans, is far smaller, the observed reduction in

marrow fat fraction in the active group was nevertheless highly significant (p=0.0003). Thus, it is likely that the two effects observed in our study—a relative increase in parameters representative of bone health and a decrease in marrow adiposity—result from the same biological process. Empirical observations suggesting that marrow fat content and bone density are inversely correlated had been reported by some of the present authors over 20 years ago, and subsequently confirmed by others [12, 56].

Some limitations of our study are noted. First, 40% and 24% of the participants randomized to the active and placebo arms, respectively, did not complete the 12-month study visit. The main reasons for the dropouts include vanishing interest, inability to comply with the protocol, undue interference with personal commitments, and newly diagnosed health issues. Other reasons were change in domicile. In some instances, no reason was given or the coordinator was unable to establish contact with the patient. The majority of dropouts occurred before the six-month visit (**Figure 2**). Since no follow-up imaging data was available, an intention-to-treat analysis was therefore not possible. Importantly, however, none of the baseline demographics, imaging, or other parameters, were significantly different ($p>0.05$) between dropouts pertaining to the two treatment arms and subjects having undergone the protocol, reassuring that no selection bias was introduced due to the dropouts. Another possible limitation is that MRI-based finite-element analysis my not be sensitive to certain possible changes in bone tissue properties, such as local mineralization and bone water. Such effects could, however, be assessed as part of an integrated examination utilizing recently developed solid-state MRI techniques [57-59]. *In vivo* image resolution is limited, typically being on the order of trabecular thickness. Nevertheless, a number of prior *in vivo* micro-MRI studies were able to detect subtle changes in bone microstructure resulting from disease progression or in response to therapy [51,

52]. Detected changes in bone parameters were relatively small. While longer-term data is still not available, it is possible that daily use of the vibration intervention beyond 12 months could potentially produce improvements in bone parameters greater than those reported in this study. Distal tibia, where MRI bone microstructure measurements were performed, is not a common osteoporotic fracture site.

Participants were not asked at the end of the study whether they could identify the type of device they were given, i.e., being able to distinguish active from placebo. However, there was no indication that subjects using placebo devices noticed the lack of the very low-amplitude vibration, due to the audible tone emitted by the device, nor was there a difference in device adherence between the two groups (see **Table 1**). While device adherence for those who completed both baseline and follow-up visits were 83% and 86% in the active and placebo arm, it would, of course be considerably lower if dropouts were included (56 and 65%, respectively). However, as pointed out before, intention to treat analysis is not possible since no data are available at the second time-point for the dropouts.

One can argue that the distal tibia is not a typical fracture site and thus must be regarded as a surrogate site, given that osteoporosis is largely a systemic disorder, implying that bone is lost across the entire skeleton (albeit to different extents). The tibial measurement site was chosen for two reasons; the first being that it is closest to the actuator generating the vibration. The second is that very high-resolution images can be obtained at this location in that the signal can be captured with closely coupled radiofrequency coils. Therefore, the resulting superior signal-to-noise ratio can be traded for improved spatial resolution (see, for instance, Wald et al. [36]). However, recent advances in imaging technology now make possible acquisition of high-

resolution images of the proximal femur, along with computational biomechanics for bone strength assessment [54].

Lastly, it is unknown whether the vibration parameters used in our study—intensity, frequency, duration, etc.—are optimal to induce the maximum response in postmenopausal women.

While the treatment effects observed after one year of vibration therapy are modest, they are nevertheless highly significant, suggesting that the intervention at least stabilizes postmenopausal bone loss. The results also shed new light on the connection between osteogenesis and adipogenesis, from the perspective of intervention involving very low-amplitude cyclical loading. The data clearly call for longer-term treatment to corroborate the present results and to determine whether the observed effects are sustained or enhanced over longer intervention periods to determine the clinical significance of the intervention. Further, porting of the technology to the most important fracture sites would be desirable and should now be possible. Follow-up studies could also examine dose response to ascertain whether increased daily duration of exposure to vibration elicits, for instance, a greater osteogenic response.

In summary, our data suggest that low-intensity vibration treatment as a preventive strategy may have potential as a non-pharmacological alternative to antiresorptive and anabolic agents, without incurring adverse side effects.

Author Contribution Statement

All authors made substantial contributions to the conception and design, acquisition, analysis, or interpretation of data, or participated in drafting of the manuscript.

References

1. MacLean, C., S. Newberry, M. Maglione, M. McMahon, V. Ranganath, M. Suttorp, W. Mojica, M. Timmer, A. Alexander, M. McNamara, S.B. Desai, A. Zhou, S. Chen, J. Carter, C. Tringale, D. Valentine, B. Johnsen, and J. Grossman, *Systematic review: comparative effectiveness of treatments to prevent fractures in men and women with low bone density or osteoporosis.* Ann Intern Med, 2008. **148**(3): p. 197-213.
2. Bauer, D.C., D. Black, K. Ensrud, D. Thompson, M. Hochberg, M. Nevitt, T. Musliner, and D. Freedholm, *Upper gastrointestinal tract safety profile of alendronate: the fracture intervention trial.* Arch Intern Med, 2000. **160**(4): p. 517-25.
3. Otto, S., M.H. Abu-Id, S. Fedele, P.H. Warnke, S.T. Becker, A. Kolk, T. Mucke, G. Mast, R. Kohnke, E. Volkmer, F. Haasters, O. Lieger, T. Iizuka, S. Porter, G. Campisi, G. Colella, O. Ploder, A. Neff, J. Wiltfang, M. Ehrenfeld, T. Kreusch, K.D. Wolff, S.R. Sturzenbaum, M. Schieker, and C. Pautke, *Osteoporosis and bisphosphonates-related osteonecrosis of the jaw: not just a sporadic coincidence--a multi-centre study.* J Craniomaxillofac Surg, 2011. **39**(4): p. 272-7.
4. Black, D.M., P.D. Delmas, R. Eastell, I.R. Reid, S. Boonen, J.A. Cauley, F. Cosman, P. Lakatos, P.C. Leung, Z. Man, C. Mautalen, P. Mesenbrink, H. Hu, J. Caminis, K. Tong, T. Rosario-Jansen, J. Krasnow, T.F. Hue, D. Sellmeyer, E.F. Eriksen, and S.R. Cummings, *Once-yearly zoledronic acid for treatment of postmenopausal osteoporosis.* N Engl J Med, 2007. **356**(18): p. 1809-22.
5. Cosman, F., D.B. Crittenden, J.D. Adachi, N. Binkley, E. Czerwinski, S. Ferrari, L.C. Hofbauer, E. Lau, E.M. Lewiecki, A. Miyauchi, C.A. Zerbini, C.E. Milmont, L. Chen, J. Maddox, P.D. Meisner, C. Libanati, and A. Grauer, *Romosozumab Treatment in Postmenopausal Women with Osteoporosis.* N Engl J Med, 2016. **375**(16): p. 1532-1543.

6. Dalsky, G.P., K.S. Stocke, A.A. Ehsani, E. Slatopolsky, W.C. Lee, and S.J. Birge, Jr., *Weight-bearing exercise training and lumbar bone mineral content in postmenopausal women.* Ann Intern Med, 1988. **108**(6): p. 824-8.

7. Sinaki, M., *Exercise and osteoporosis.* Arch Phys Med Rehabil, 1989. **70**(3): p. 220-9.

8. David, V., A. Martin, M.H. Lafage-Proust, L. Malaval, S. Peyroche, D.B. Jones, L. Vico, and A. Guignandon, *Mechanical loading down-regulates peroxisome proliferator-activated receptor gamma in bone marrow stromal cells and favors osteoblastogenesis at the expense of adipogenesis.* Endocrinology, 2007. **148**(5): p. 2553-62.

9. Rubin, C.T., E. Capilla, Y.K. Luu, B. Busa, H. Crawford, D.J. Nolan, V. Mittal, C.J. Rosen, J.E. Pessin, and S. Judex, *Adipogenesis is inhibited by brief, daily exposure to high-frequency, extremely low-magnitude mechanical signals.* Proc Natl Acad Sci U S A, 2007. **104**(45): p. 17879-84.

10. Di Iorgi, N., S.D. Mittelman, and V. Gilsanz, *Differential effect of marrow adiposity and visceral and subcutaneous fat on cardiovascular risk in young, healthy adults.* Int J Obes (Lond), 2008. **32**(12): p. 1854-60.

11. Wehrli, F.W., J.A. Hopkins, S.N. Hwang, H.K. Song, P.J. Snyder, and J.G. Haddad, *Cross-sectional study of osteopenia with quantitative MR imaging and bone densitometry.* Radiology, 2000. **217**(2): p. 527-38.

12. Yeung, D.K., J.F. Griffith, G.E. Antonio, F.K. Lee, J. Woo, and P.C. Leung, *Osteoporosis is associated with increased marrow fat content and decreased marrow fat unsaturation: a proton MR spectroscopy study.* J Magn Reson Imaging, 2005. **22**(2): p. 279-85.

13. Jankovich, J.P., *The effects of mechanical vibration on bone development in the rat.* J Biomech, 1972. **5**(3): p. 241-50.

14. Rubin, C., A.S. Turner, S. Bain, C. Mallinckrodt, and K. McLeod, *Anabolism. Low mechanical signals strengthen long bones.* Nature, 2001. **412**(6847): p. 603-4.

15. Tezval, M., M. Biblis, S. Sehmisch, U. Schmelz, L. Kolios, T. Rack, K.M. Stuermer, and E.K. Stuermer, *Improvement of femoral bone quality after low-magnitude, high-frequency mechanical stimulation in the ovariectomized rat as an osteopenia model.* Calcif Tissue Int, 2011. **88**(1): p. 33-40.

16. Rubin, C., R. Recker, D. Cullen, J. Ryaby, J. McCabe, and K. McLeod, *Prevention of postmenopausal bone loss by a low-magnitude, high-frequency mechanical stimuli: a clinical trial assessing compliance, efficacy, and safety.* J Bone Miner Res, 2004. **19**(3): p. 343-51.

17. Lau, E., S. Al-Dujaili, A. Guenther, D. Liu, L. Wang, and L. You, *Effect of low-magnitude, high-frequency vibration on osteocytes in the regulation of osteoclasts.* Bone, 2010. **46**(6): p. 1508-15.

18. Arnsdorf, E.J., P. Tummala, A.B. Castillo, F. Zhang, and C.R. Jacobs, *The epigenetic mechanism of mechanically induced osteogenic differentiation.* J Biomech, 2010. **43**(15): p. 2881-6.

19. Robling, A.G., P.J. Niziolek, L.A. Baldridge, K.W. Condon, M.R. Allen, I. Alam, S.M. Mantila, J. Gluhak-Heinrich, T.M. Bellido, S.E. Harris, and C.H. Turner, *Mechanical stimulation of bone in vivo reduces osteocyte expression of Sost/sclerostin.* J Biol Chem, 2008. **283**(9): p. 5866-75.

20. Rubin, C., A.S. Turner, R. Muller, E. Mittra, K. McLeod, W. Lin, and Y.X. Qin, *Quantity and quality of trabecular bone in the femur are enhanced by a strongly anabolic, noninvasive mechanical intervention.* J Bone Miner Res, 2002. **17**(2): p. 349-57.

21. Judex, S., S. Boyd, Y.X. Qin, S. Turner, K. Ye, R. Muller, and C. Rubin, *Adaptations of trabecular bone to low magnitude vibrations result in more uniform stress and strain under load.* Ann Biomed Eng, 2003. **31**(1): p. 12-20.

22. Hannan, M.T., D.M. Cheng, E. Green, C. Swift, C.T. Rubin, and D.P. Kiel, *Establishing the compliance in elderly women for use of a low level mechanical stress device in a clinical osteoporosis study.* Osteoporos Int, 2004. **15**(11): p. 918-26.

23. Gilsanz, V., T.A. Wren, M. Sanchez, F. Dorey, S. Judex, and C. Rubin, *Low-level, high-frequency mechanical signals enhance musculoskeletal development of young women with low BMD.* J Bone Miner Res, 2006. **21**(9): p. 1464-74.

24. Verschueren, S.M., M. Roelants, C. Delecluse, S. Swinnen, D. Vanderschueren, and S. Boonen, *Effect of 6-month whole body vibration training on hip density, muscle strength, and postural control in postmenopausal women: a randomized controlled pilot study.* J Bone Miner Res, 2004. **19**(3): p. 352-9.

25. Ward, K., C. Alsop, J. Caulton, C. Rubin, J. Adams, and Z. Mughal, *Low magnitude mechanical loading is osteogenic in children with disabling conditions.* J Bone Miner Res, 2004. **19**(3): p. 360-9.

26. Lam, T.P., B.K. Ng, L.W. Cheung, K.M. Lee, L. Qin, and J.C. Cheng, *Effect of whole body vibration (WBV) therapy on bone density and bone quality in osteopenic girls with adolescent idiopathic scoliosis: a randomized, controlled trial.* Osteoporos Int, 2013. **24**(5): p. 1623-36.

27. Wren, T.A., D.C. Lee, R. Hara, S.A. Rethlefsen, R.M. Kay, F.J. Dorey, and V. Gilsanz, *Effect of high-frequency, low-magnitude vibration on bone and muscle in children with cerebral palsy.* J Pediatr Orthop, 2010. **30**(7): p. 732-8.

28. Judex, S., L.R. Donahue, and C. Rubin, *Genetic predisposition to low bone mass is paralleled by an enhanced sensitivity to signals anabolic to the skeleton.* Faseb J, 2002. **16**(10): p. 1280-2.

29. Kiel, D.P., M.T. Hannan, B.A. Barton, M.L. Bouxsein, E. Sisson, T. Lang, B. Allaire, D. Dewkett, D. Carroll, J. Magaziner, E. Shane, E.T. Leary, S. Zimmerman, and C.T. Rubin, *Low-Magnitude Mechanical Stimulation to Improve Bone Density in Persons of Advanced Age: A Randomized, Placebo-Controlled Trial.* J Bone Miner Res, 2015. **30**(7): p. 1319-28.

30. Fratini, A., T. Bonci, and A.M. Bull, *Whole Body Vibration Treatments in Postmenopausal Women Can Improve Bone Mineral Density: Results of a Stimulus Focussed Meta-Analysis.* PLoS One, 2016. **11**(12): p. e0166774.

31. Leonard, M.B., J. Shults, J. Long, R.N. Baldassano, J.K. Brown, K. Hommel, B.S. Zemel, S. Mahboubi, K. Howard Whitehead, R. Herskovitz, D. Lee, J. Rausch, and C.T. Rubin, *Effect of Low-Magnitude Mechanical Stimuli on Bone Density and Structure in Pediatric Crohn's Disease: A Randomized Placebo-Controlled Trial.* J Bone Miner Res, 2016. **31**(6): p. 1177-88.

32. Rajapakse, C.S., E.A. Kobe, A.S. Batzdorf, M.W. Hast, and F.W. Wehrli, *Accuracy of MRI-based finite element assessment of distal tibia compared to mechanical testing.* Bone, 2018. **108**: p. 71-78.

33. Rajapakse, C.S., M.B. Leonard, E.A. Kobe, M.A. Slinger, K.A. Borges, E. Billig, C.T. Rubin, and F.W. Wehrli, *The Efficacy of Low-intensity Vibration to Improve Bone Health in Patients with End-stage Renal Disease Is Highly Dependent on Compliance and Muscle Response.* Acad Radiol, 2017. **24**(11): p. 1332-1342.

34. Fritton, J.C., C.T. Rubin, Y.X. Qin, and K.J. McLeod, *Whole-body vibration in the skeleton: development of a resonance-based testing device.* Ann Biomed Eng, 1997. **25**(5): p. 831-9.

35. Baum, T., A. Rohrmeier, J. Syvari, M.N. Diefenbach, D. Franz, M. Dieckmeyer, A. Scharr, H. Hauner, S. Ruschke, J.S. Kirschke, and D.C. Karampinos, *Anatomical Variation of Age-Related Changes in Vertebral Bone Marrow Composition Using Chemical Shift Encoding-Based Water-Fat Magnetic Resonance Imaging.* Front Endocrinol (Lausanne), 2018. **9**: p. 141.

36. Wald, M.J., J.F. Magland, C.S. Rajapakse, and F.W. Wehrli, *Structural and mechanical parameters of trabecular bone estimated from in vivo high-resolution magnetic resonance images at 3 tesla field strength.* J Magn Reson Imaging, 2010. **31**(5): p. 1157-68.

37. Rajapakse, C.S., J.F. Magland, and F.W. Wehrli, *Fast prospective registration of in vivo MR images of trabecular bone microstructure in longitudinal studies.* Magn Reson Med, 2008. **59**(5): p. 1120-6.

38. Ma, J., F.W. Wehrli, and H.K. Song, *Fast 3D large-angle spin-echo imaging (3D FLASE).* Magn Reson Med, 1996. **35**(6): p. 903-10.

39. Mostoufi-Moab, S., J. Magland, E.J. Isaacoff, W. Sun, C.S. Rajapakse, B. Zemel, F. Wehrli, K. Shekdar, J. Baker, J. Long, and M.B. Leonard, *Adverse Fat Depots and*

Marrow Adiposity Are Associated With Skeletal Deficits and Insulin Resistance in Long-Term Survivors of Pediatric Hematopoietic Stem Cell Transplantation. J Bone Miner Res, 2015. **30**(9): p. 1657-66.

40. Rajapakse, C.S., J.F. Magland, M.J. Wald, X.S. Liu, X.H. Zhang, X.E. Guo, and F.W. Wehrli, *Computational biomechanics of the distal tibia from high-resolution MR and micro-CT images.* Bone, 2010. **47**(3): p. 556-63.
41. Magland, J.F., N. Zhang, C.S. Rajapakse, and F.W. Wehrli, *Computationally-optimized bone mechanical modeling from high-resolution structural images.* PLoS One, 2012. **7**(4): p. e35525.
42. Wehrli, F.W., B.R. Gomberg, P.K. Saha, H.K. Song, S.N. Hwang, and P.J. Snyder, *Digital topological analysis of in vivo magnetic resonance microimages of trabecular bone reveals structural implications of osteoporosis.* J Bone Miner Res, 2001. **16**(8): p. 1520-31.
43. Rajapakse, C.S., E.A. Phillips, W. Sun, M. Wald, J. Snyder, X.E. Guo, and F.W. Wehrli. *Vertebral deformity fracture number and severity are associated with mechanical competence at peripheral bone derived by micro-MRI based biomechanics*. in *ASBMR*. 2012.
44. Baker, J.F., M. Davis, R. Alexander, B.S. Zemel, S. Mostoufi-Moab, J. Shults, M. Sulik, D.J. Schiferl, and M.B. Leonard, *Associations between body composition and bone density and structure in men and women across the adult age spectrum.* Bone, 2013. **53**(1): p. 34-41.
45. Adams JE, E.K., Zemel BS, Ward KA., *Quantitative Computer Tomography in Children and Adolescents: The 2013 ISCD Pediatric Official Positions.* Journal of Clinical

Densitometry: Assessment & Management of Musculoskeletal Health, 2014. **17**(2): p. 258-274.

46. Shepherd, J.A., L. Wang, B. Fan, V. Gilsanz, H.J. Kalkwarf, J. Lappe, Y. Lu, T. Hangartner, B.S. Zemel, M. Fredrick, S. Oberfield, and K.K. Winer, *Optimal monitoring time interval between DXA measures in children.* J Bone Miner Res, 2011. **26**(11): p. 2745-52.

47. Lam, S.C., M.J. Wald, C.S. Rajapakse, Y. Liu, P.K. Saha, and F.W. Wehrli, *Performance of the MRI-based virtual bone biopsy in the distal radius: serial reproducibility and reliability of structural and mechanical parameters in women representative of osteoporosis study populations.* Bone, 2011. **49**(4): p. 895-903.

48. Afzal, S.Y., A.R. Wender, M.D. Jones, E.B. Fung, and E.L. Pico, *The effect of low magnitude mechanical stimulation (LMMS) on bone density in patients with Rett syndrome: a pilot and feasibility study.* J Pediatr Rehabil Med, 2014. **7**(2): p. 167-78.

49. Mogil, R.J., S.C. Kaste, R.J. Ferry, Jr., M.M. Hudson, D.A. Mulrooney, C.R. Howell, R.E. Partin, D.K. Srivastava, L.L. Robison, and K.K. Ness, *Effect of Low-Magnitude, High-Frequency Mechanical Stimulation on BMD Among Young Childhood Cancer Survivors: A Randomized Clinical Trial.* JAMA Oncol, 2016. **2**(7): p. 908-914.

50. Slatkovska, L., S.M. Alibhai, J. Beyene, H. Hu, A. Demaras, and A.M. Cheung, *Effect of 12 months of whole-body vibration therapy on bone density and structure in postmenopausal women: a randomized trial.* Ann Intern Med, 2011. **155**(10): p. 668-79, W205.

51. Rajapakse, C.S., M.B. Leonard, Y.A. Bhagat, W. Sun, J.F. Magland, and F.W. Wehrli, *Micro-MR imaging-based computational biomechanics demonstrates reduction in*

cortical and trabecular bone strength after renal transplantation. Radiology, 2012. **262**(3): p. 912-20.

52. Folkesson, J., J. Goldenstein, J. Carballido-Gamio, G. Kazakia, A.J. Burghardt, A. Rodriguez, R. Krug, A.E. de Papp, T.M. Link, and S. Majumdar, *Longitudinal evaluation of the effects of alendronate on MRI bone microarchitecture in postmenopausal osteopenic women.* Bone, 2011. **48**(3): p. 611-21.

53. Wehrli, F.W., C.S. Rajapakse, J.F. Magland, and P.J. Snyder, *Mechanical implications of estrogen supplementation in early postmenopausal women.* J Bone Miner Res, 2010. **25**(6): p. 1406-14.

54. Chang, G., S. Honig, R. Brown, C.M. Deniz, K.A. Egol, J.S. Babb, R.R. Regatte, and C.S. Rajapakse, *Finite element analysis applied to 3-T MR imaging of proximal femur microarchitecture: lower bone strength in patients with fragility fractures compared with control subjects.* Radiology, 2014. **272**(2): p. 464-74.

55. Hilaire, L., F.W. Wehrli, and H.K. Song, *High-speed spectroscopic imaging for cancellous bone marrow R(2)* mapping and lipid quantification.* Magn Reson Imaging, 2000. **18**(7): p. 777-86.

56. Wehrli, F.W., J.A. Hopkins, S.N. Hwang, H.K. Song, P.J. Snyder, and J.G. Haddad, *Cross-sectional study of osteopenia by quantitative magnetic resonance and bone densitometry.* Radiology, 2000. **217**: p. 527-538.

57. Rajapakse, C.S., M. Bashoor-Zadeh, C. Li, W. Sun, A.C. Wright, and F.W. Wehrli, *Volumetric Cortical Bone Porosity Assessment with MR Imaging: Validation and Clinical Feasibility.* Radiology, 2015. **276**(2): p. 526-35.

58. Zhao, X., H.K. Song, A.C. Seifert, C. Li, and F.W. Wehrli, *Correction: Feasibility of assessing bone matrix and mineral properties in vivo by combined solid-state 1H and 31P MRI.* PLoS One, 2018. **13**(1): p. e0192186.

59. Techawiboonwong, A., H.K. Song, M.B. Leonard, and F.W. Wehrli, *Cortical bone water: in vivo quantification with ultrashort echo-time MR imaging.* Radiology, 2008. **248**(3): p. 824-33.

***Table 1**: Patient characteristics and adherence. Unless noted, values are mean ± SD or median (interquartile range) for normally and non-normally distributed data, respectively, based on per-protocol analysis.*

Parameter	**Active**	**Placebo**	***p***
n	42	38	
Age, years	61 (55.2 – 63.4)	58 (54.5 – 62.1)	0.45
Age at menopause, years	50 (46.0 – 54.8)	51 (49.1 – 53.5)	0.80
Weight, kg	69.4 ± 10.00	68.2 ± 9.78	0.61
Height, m	1.63 ± 0.066	1.64 ± 0.066	0.38
BMI, kg/m^2	26.2 ± 3.62	25.3 ± 3.55	0.27
Waist circumference, cm	98.0 (89.0 – 102)	93.5 (88.8 – 102)	0.86
Total hip BMD T-score	-0.75 (-1.13 – -0.275)	-0.70 (-1.03 – 0.45)	0.26
Spine BMD T-score	-0.70 (-1.48 – -0.193)	-1.05 (-1.63 – -0.300)	0.36
Race, count			
White	27	26	
Black	10	10	
Asian	2		
Multiracial	2	2	
Undisclosed	1		
Adherence (per-protocol), %	83.0 (62.3 – 91.1)	86.1 (63.1 – 93.2)	0.72
Adherence (intention-to-treat), %	78.4 (0.02 – 88.7)	74.8 (53.1 – 91.3)	0.38

***Table 2**: Percent changes in outcome parameters between baseline and 12-month follow up, in the active group versus the placebo group. Unless noted, values are mean ± SD or median (interquartile range) for normally and non-normally distributed data, respectively. Bold text indicates significance at* p*<0.05. BV/TV = bone volume fraction; vBMD = volumetric bone mineral density; aBMD = areal bone mineral density.*

Parameter	**Active % Change**	**Placebo % Change**	***p***
Distal Tibia			
Stiffness	1.31 ± 6.05	-2.55 ± 3.90	**0.01**
BV/TV	1.12 ± 5.70	-2.14 ± 5.79	**0.048**
Surface/Curve	4.58 ± 11.8	1.27 ± 9.79	0.28
Erosion Index	-5.09 ± 8.87	0.26 ± 9.60	**0.04**
Trabecular vBMD	0.64 (-0.20 – 2.21)	0.13 (-1.22 – 0.84)	**0.02**
Mid Tibia			
Cortical vBMD	-0.10 ± 0.63	0.04 ± 0.63	0.41
Hip			
Total aBMD	-0.42 ± 1.85	-0.79 ± 1.84	0.47
Spine			
Fat Fraction	-1.25 ± 1.36	0.34 ± 3.05	**0.03**
aBMD	-0.47 ± 2.64	0.13 ± 2.99	0.43
Deformity	0.04 ± 2.39	-0.22 ± 1.41	0.66

***Table 3**: Within-group changes between baseline and follow-up parameters. Unless noted, values are mean ± SD or median (interquartile range) for normally and non-normally distributed data, respectively. Bold text indicates significance at* $p<0.05$. *BV/TV = bone volume fraction; vBMD = volumetric bone mineral density; aBMD = areal bone mineral density.*

Parameter	Modality	Active			Placebo		
		Month 0	Month 12	*p*	Month 0	Month 12	*p*
Distal Tibia							
Stiffness (GPa)	MRI	1.39 (1.31-1.64)	1.39 (1.34-1.60)	0.54	1.37 (1.26-1.66)	1.35 (1.25-1.65)	**0.004**
BV/TV	MRI	0.108 (0.103-0.115)	0.110 (0.104-0.114)	0.72	0.106 (0.100-0.113)	0.105 (0.099-0.109)	0.06
Surface/Curve	MRI	6.70 ± 0.87	6.96 ± 0.90	0.06	6.32 ± 1.05	6.34 0.77	0.55
Erosion Index	MRI	0.71 ± 0.09	0.67 ± 0.08	**0.004**	0.75 ± 0.13	0.74 ± 0.11	0.52
Trabecular vBMD (mg/cc)	pQCT	230 ± 29.6	232 ± 29.2	0.08	220 ± 31.9	219 ± 32.6	0.43
Mid Tibia							
Cortical vBMD (mg/cc)	pQCT	1150 ± 34.9	1148 ± 34.5	0.43	1143 ± 37.0	1143 ± 35.2	0.76
Hip							
Total aBMD (mg/cc)	DXA	856 (803-947)	855 (803-948)	0.12	863 (803-990)	858 (828-1003)	**0.02**
Spine							
Fat Fraction (%)	MRI	70.0 ± 5.30	69.0 ± 4.96	**0.0003**	67.3 ± 5.95	67.4 ± 6.05	0.71
Deformity	MRI	1.46 ± 2.58	2.36 ± 2.39	0.35	1.44 ± 2.01	1.13 ± 1.95	0.88
aBMD (mg/cc)	DXA	964 ± 104	959 ± 105	0.34	960 ± 115	961 ± 113	0.92

***Table 4**: Associations between baseline measurements and percent change in primary outcome variable, i.e., distal tibia stiffness. Bold text indicates significance at* p*<0.05. BV/TV = bone volume fraction; vBMD = volumetric bone mineral density; aBMD = areal bone mineral density.*

Parameter	Modality	Active		Placebo		Group Difference
		R	*p*	R	*p*	*p*
Distal Tibia						
Stiffness	MRI	-0.58	**0.002**	0.09	0.66	**0.01**
BV/TV	MRI	-0.52	**0.01**	-0.32	0.12	0.41
Surface/Curve	MRI	-0.48	**0.01**	-0.10	0.62	0.16
Erosion Index	MRI	0.47	**0.02**	0.11	0.62	0.18
Trabecular vBMD	pQCT	-0.34	0.09	-0.07	0.73	0.35
Mid Tibia						
Cortical vBMD	pQCT	-0.17	0.40	-0.36	0.08	0.49
Hip						
Total aBMD	DXA	-0.40	**0.045**	-0.19	0.35	0.45
Spine						
Fat Fraction	MRI	0.48	**0.02**	-0.13	0.54	**0.03**
Deformity	MRI	-0.04	0.86	-0.22	0.32	0.57
aBMD	DXA	-0.44	**0.03**	0.41	**0.04**	**0.002**

Fig 1: Illustration of the low-intensity vibration intervention, as well as the MRI, pQCT, and DXA measurement sites. For details, see text. DXA = dual-energy X-ray absorptiometry; BMD = bone mineral density; pQCT = peripheral computed quantitative tomography; LIV = low-intensity vibration.

Fig 2. CONSORT flow diagram for the study. DXA = dual-energy X-ray absorptiometry; BMI = body mass index.

Fig 3: MR-derived bone volume fraction maps of the distal tibia of a representative participant taken 12 months apart show the ability to capture matching bone microstructure using prospective registration. Regions are magnified to demonstrate matched pairs. These 3D maps serve as input into the finite-element model, yielding a measure of stiffness in GPa, and thus strength.

Fig 4: Percent temporal changes in parameters in active and placebo groups. Significant group differences are indicated by *p* values. BV/TV = bone volume fraction; vBMD = volumetric bone mineral density; aBMD = areal bone mineral density.

Fig 5: Differential effects of baseline stiffness on change in stiffness in the active versus placebo arms.

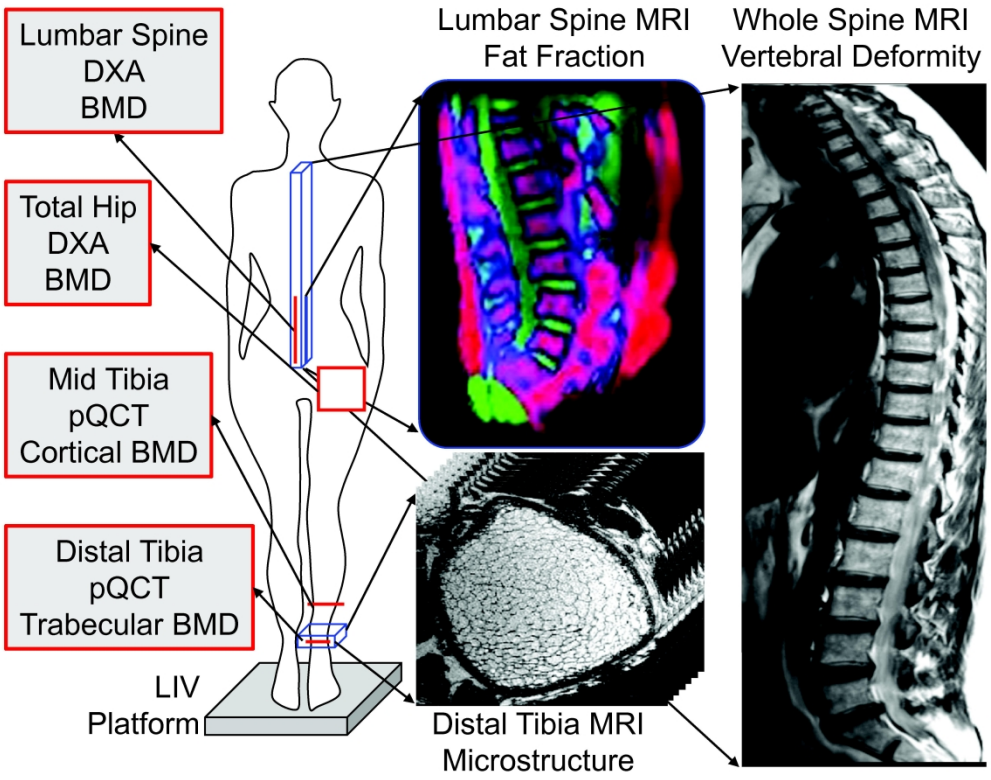

Fig 1: Illustration of the low-intensity vibration intervention, as well as the MRI, pQCT, and DXA measurement sites. For details, see text. DXA = dual-energy X-ray absorptiometry; BMD = bone mineral density; pQCT = peripheral computed quantitative tomography; LIV = low-intensity vibration.

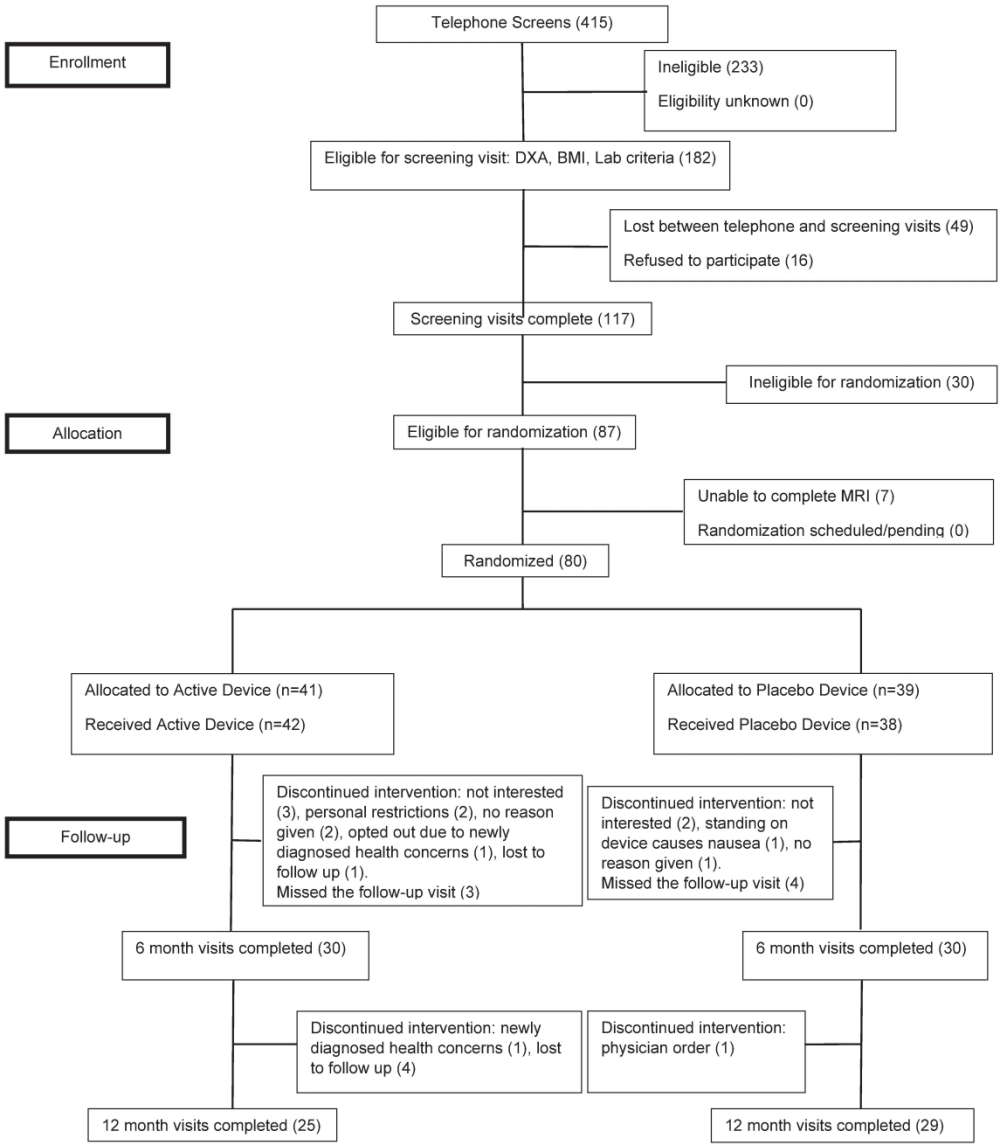

Fig 2: CONSORT flow diagram for the study. DXA = dual-energy X-ray absorptiometry; BMI = body mass index.

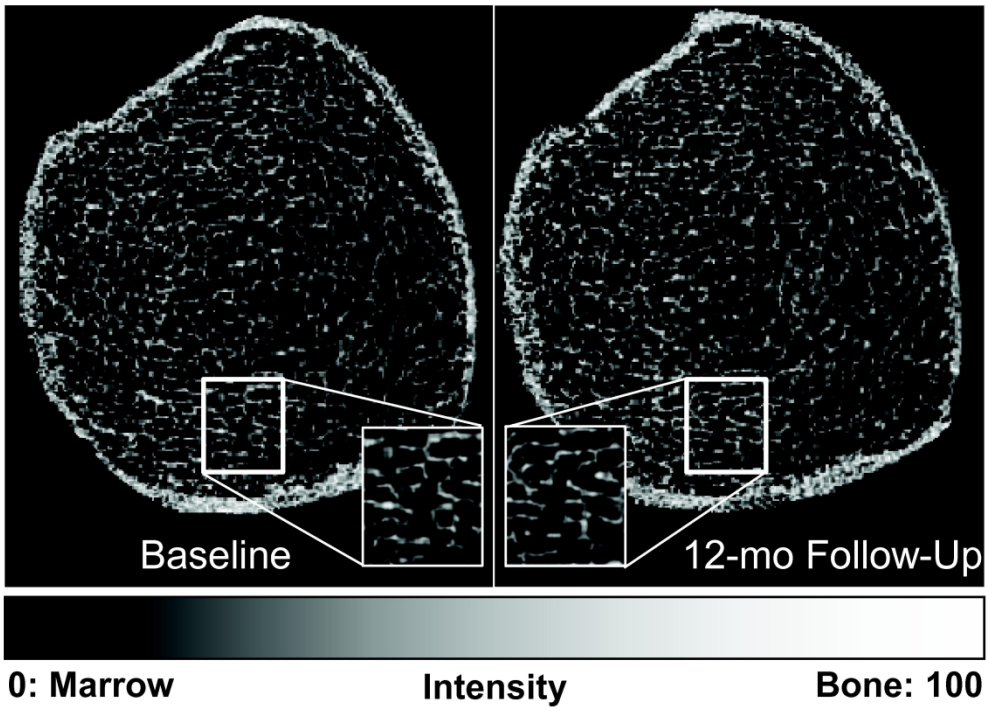

Fig 3: MR-derived bone volume fraction maps of the distal tibia of a representative participant taken 12 months apart show the ability to capture matching bone microstructure using prospective registration. Regions are magnified to demonstrate matched pairs. These 3D maps serve as input into the finite-element model, yielding a measure of stiffness in GPa, and thus strength.

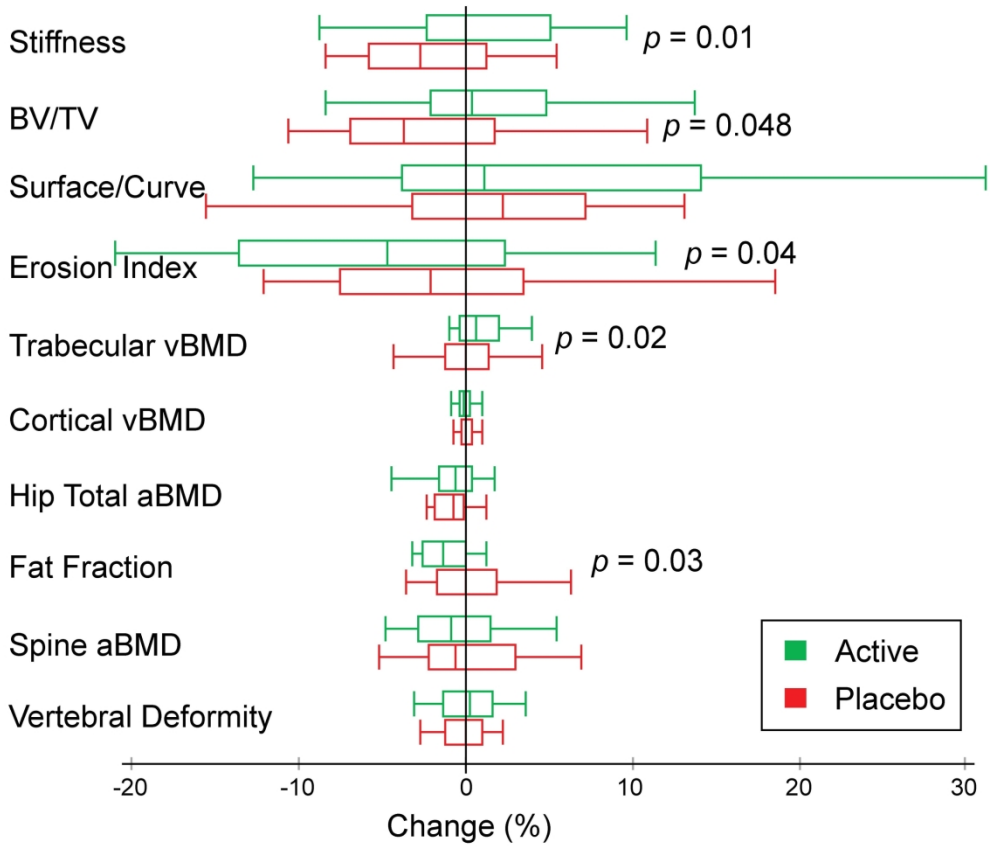

Fig 4: Percent temporal changes in parameters in active and placebo groups. Significant group differences are indicated by p values. BV/TV = bone volume fraction; vBMD = volumetric bone mineral density; aBMD = areal bone mineral density.

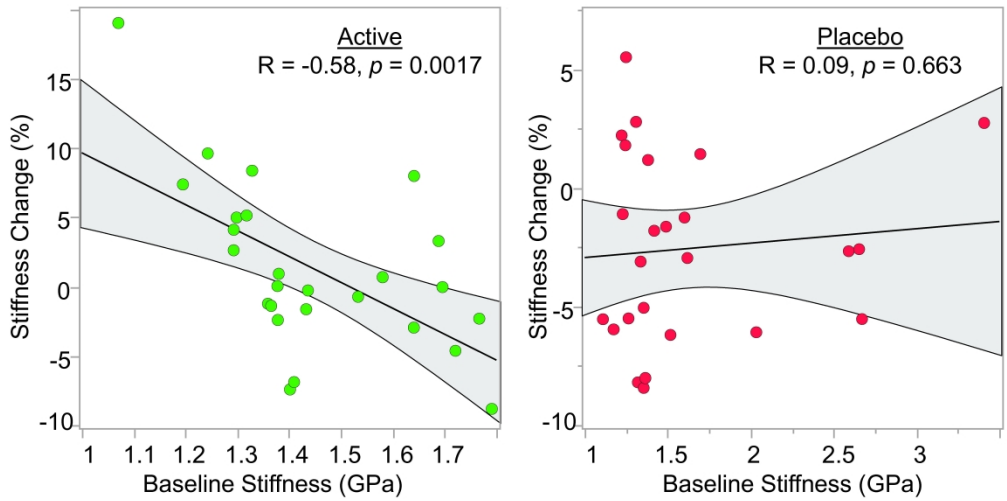

Fig 5: Differential effects of baseline stiffness on change in stiffness in the active versus placebo arms.